Integrated platform to assess seismic resilience at the community level

Marasco, Sebastiano; Cardoni, Alessandro; Zamani Noori, Ali; Kammouh, Omar; Domaneschi, Marco; Cimellarof, Gian Paolo

DOI
10.1016/j.scs.2020.102506

Publication date
2021

Document Version
Accepted author manuscript

Published in
Sustainable Cities and Society

Citation (APA)
Marasco, S., Cardoni, A., Zamani Noori, A., Kammouh, O., Domaneschi, M., & Cimellarof, G. P. (2021). Integrated platform to assess seismic resilience at the community level. *Sustainable Cities and Society*, *64*, 1-20. Article 102506. https://doi.org/10.1016/j.scs.2020.102506

Integrated platform to assess seismic resilience at the community level

Abstract: Due to the increasing frequency of disastrous events, the challenge of creating large-scale simulation models has become of major significance. Indeed, several simulation strategies and methodologies have been recently developed to explore the response of communities to natural disasters. Such models can support decision-makers during emergency operations allowing to create a global view of the emergency identifying consequences. An integrated platform that implements a community hybrid model with real-time simulation capabilities is presented in this paper. The platform's goal is to assess seismic resilience and vulnerability of critical infrastructures (e.g., built environment, power grid, socio-technical network) at the urban level, taking into account their interdependencies.

Finally, different seismic scenarios have been applied to a large-scale virtual city model. The platform proved to be effective to analyze the emergency and could be used to implement countermeasures that improve community response and overall resilience.

Keywords: disaster resilience, urban community, interdependence analysis, critical infrastructure, damage assessment, multiprocessing.

LIST OF AABBREVIATION

RTN: Road Transportation Network

WDN: Water Distribution Network

PG: Power Grid

STN: Socio-Technical Network

RV: Random Variable

MCS: Monte Carlo Simulation

RC: Reinforced Concrete

CPU: Central Processing Unit

GPU: Graphical Processing Unit

RF: Random Forest

KNR: k-Nearest Neighbors

DDM: Density Design Method

ABM: Agent Based Model

DS: Damage State

SC: Single-Core

MC: Multi-Core

1. INTRODUCTION

Recent natural and manmade disasters demonstrated the high vulnerability and unpreparedness of most communities (Alsubaie et al., 2015). Modern societies have proved to be heavily dependent on their critical infrastructures, which provide essential services and

contribute significantly to the social and economic development (Ismail et al., 2011). Having a more comprehensive insight into critical infrastructures and their mutual dependencies would yield crucial information on community disaster vulnerability, which represents the sensitivity of a community exposed to a given hazardous event (Cash et al., 2006).

Understanding the vulnerability of critical infrastructures is of paramount importance as it allows to properly predict community resilience, which is defined as the ability of a system to respond and recover from disaster (Cimellaro et al., 2016; Cutter et al., 2008). Among all definitions of resilience, (Walker & Salt, 2006) define resilient systems as "sustaining ecosystems and people in a changing world", therefore resilience is intertwined with sustainability. Resilience can be considered as one of the indicators of sustainability as being resilient is essential for being sustainable (G. P. Cimellaro, 2016).

Current practices of infrastructure modeling incorporate both facilities (housing, commercial, and cultural facilities) and lifelines (hospitals, transportation systems, power and communication networks, water distribution networks, etc.) (Renschler et al., 2010). However, there is still a lack of tools and methods to assess resilience at the urban level (Ribeiro & Gonçalves, 2019).

The first step towards large-scale urban simulations is the development of standards and metrics that enable decision-makers to quantify resilience. An indicator-based framework for measuring urban community resilience was introduced by Kammouh et al. (2019). The framework, namely *PEOPLES*, captures the overall resilience of communities considering different aspects/layers, i.e., population, environmental and ecosystem, organized governmental services, physical infrastructures, lifestyle, economic development, and social

capital. Karakoc et al. (2020) proposed an important measure that is derived by social aspects of resilience to identify the most critical components that have the largest impact on the performance of interdependent networks. A hybrid simulation framework was suggested by Hwang et al. (2016) to plan immediate recovery measures for the regional facilities in the aftermath of a disaster combining system dynamic approaches with discrete-event simulations. More detailed indicator-based models have been developed for single infrastructures typical of modern communities. For instance, Balaei et al. (2020) identified indicators to quantify the robustness and consequently the resilience of water supply systems, which are essential in the aftermath of a disaster.

The interaction among critical infrastructures needs to be examined to correctly model and comprehensively analyze the community system. A modeling and simulation framework was developed by Dudenhoeffer et al. (2006) to simulate the urban infrastructure interdependencies given a flood event. Infrastructures were modeled as a network consisting of nodes and edges, while interdependencies were defined as direct links between infrastructures' components. Focusing on system interdependencies and related cascading effects, Guidotti et al. (2016) investigated the effects of the seismic damage of an electric power network on a water distribution network while Domaneschi et al. (2019) focused on the interdependency between seismic damage of masonry buildings and transportation networks. In addition, a recent study showed the importance of considering the pre-event conditions of interdependent stormwater drainage system and road transportation network (Yang et al., 2019).

Recent years have seen a rise in the development of integrated platforms to quantify the resilience of infrastructure systems. In their research, Repetto et al. (2017) provided tools for

real-time monitoring of seaports which can have a highly positive impact on improving the resilience of coastal urban communities. Different applications can be found for different scenarios and hazards. Among others, a conceptual integrated framework (Martí, 2014) was proposed to plan and coordinate the response of multiple infrastructures during disasters. Borgdorff et al. (2015) developed a software tool (SIM-CITY) to predict complex urban dynamics to coordinate emergency services and urban planners. An example of a Virtual Geographic Environment (VGE)-based simulation framework for flood disaster management was presented by Ding et al. (2014), while a community-driven project named Global Earthquake Model (GEM) (Crowley et al., 2013) simulates earthquake risks. The main goal of the GEM foundation is to define standards and collect best practices related to seismic hazard and risk assessment methodologies, with a focus on data collection and storage. Besides, seismic vulnerability through empirical, analytical, and expert opinion was addressed by Porter et al. (2012), while an open-source software named the OpenQuake (Silva et al., 2014) was developed to evaluate human or economic losses.

Although previous studies have tackled disaster community modeling and simulation, the integration of all computing resources into a unified platform remains a challenge. An integrated platform would provide a more effective problem-solving approach that is useful to assist the decision support system. This poses several practical challenges in enabling different simulators to interact and in organizing the information system flow for a standardized output.

The main objective of this work is to develop an integrated platform to assess seismic resilience at the community level. With this aim, new methods and computational procedures are proposed. These methods are implemented in a new software tool that assesses the

vulnerability of critical infrastructures in large-scale urban areas. Besides, innovative physical interdependency models have been implemented in the platform. As a testbed, a virtual city that mimics a typical Italian building stock is designed. The information of the physical systems (i.e. buildings, transportation, power, water networks) is collected in the form of a machine-readable database. The designed testbed is used throughout the manuscript to explain the different methodologies introduced in this paper; thus, there will not be a separate section dedicated to the methodologies.

The entire analysis is controlled in a Python-based environment implementing a parallel computing workflow. The developed software comprises different Python classes that include all necessary algorithms to assess the building portfolio damage and model the physical interdependencies within and across the networks. The software tool includes visualization methods that convert the numerical results into easy-to-interpret figures which can be crucial for decision-makers. Resilience and interdependency analyses, which this paper is centered around, help decision-makers to identify vulnerable structures and infrastructure prior to the event so they can develop sustainable technologies for preparedness and reconstruction.

The rest of the paper is organized as follows. Section 2 gives an overview of the proposed hybrid community model. Section 3 presents the details for modeling and simulating the building portfolio. Section 4 describes the methods used for modeling the road infrastructure network and for analyzing its interdependency with the building stock. Sections 5 and 6 deal with the power system and water distribution network, respectively. In section 7, the agent-based model used to simulate the socio-technical network is introduced. Section 8 presents an application of the entire computational procedure considering different seismic scenarios to

demonstrate the platform's features and functionality. Finally, conclusions are drawn in Section 9.

2. HYBRID COMMUNITY MODEL

Community vulnerability modeling is multi-layered as it considers the responses of different infrastructures and social networks, including their interdependencies (Pamungkas et al., 2014). Common approaches can be grouped into six types: empirical, agent-based, system dynamics, economic theory-based, network, and others (Ouyang, 2014). Empirical approaches analyze the system's components according to historical disaster data. In agent-based approaches, the system is considered as adaptive and its complex behavior is described as the interaction of autonomous agents (Cimellaro et al., 2017). System dynamic approaches attempt to model the evolutionary behavior of interdependent infrastructures by capturing causes and effects under an external impact. On the other hand, network-based approaches model each infrastructure combining nodes and links, while the interdependencies among infrastructures are defined using interlinks. Finally, economic theory-based approaches focus on market rules to model interdependencies. Other approaches include Bayesian networks, hierarchical methods, and hybrid models. The latter result from a combination of two or more traditional methods (Kammouh, Noori, et al., 2018).

In this work, a hybrid model is proposed to couple Network Models (NMs), which are used to analyze the physical infrastructures, with Agent-Based Models (ABMs) to simulate the socio-technical networks (emergency rescue services, firefighters, etc.). It is applied to a virtual city named *Ideal City*, which is envisioned as being representative of a typical European urban area and it is inspired by the city of Turin in Italy. Its building portfolio comprises four different

sectors including housing (residential building, hotel, shelter), education (school, university, library), business (shopping centers, retail stores, heavy industries), and public services (hospital, police station, churches, airport, etc.). Figure 1 schematically shows the hybrid multi-layered model of *Ideal City* and the interdependencies among the networks. Four lifelines supporting the community's demands are modeled: (i) the Road Transportation Network (RTN), (ii) the Water Distribution Network (WDN), (iii) the Power Grid (PG), and (iv) the Socio-Technical Network (STN). The proposed hybrid model takes into account also cascading effects between the building damage and the RTN, the PG, the WDN, and the STN in the aftermath of an earthquake.

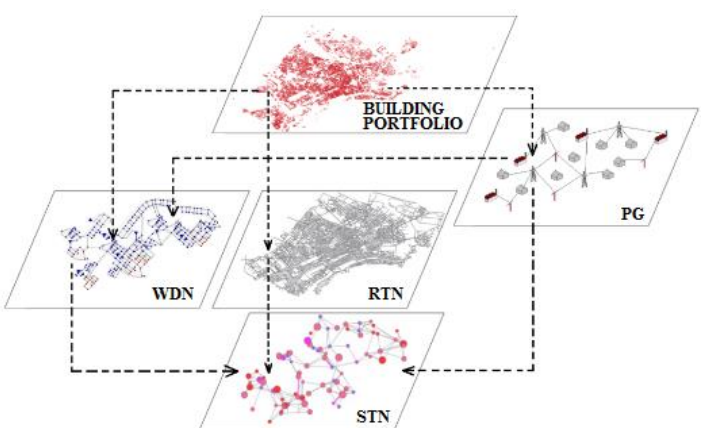

Figure 1. Hybrid multi-layered model and interdependencies (dashed arrows).

The dashed lines refer to the interdependencies between layers that have been modeled in the proposed platform. The damage experienced by the building portfolio is considered as the trigger event inducing an additional loss of functionality in all the remaining networks (RTN, WDN, PG, and STN). Moreover, the functionality of WDN is dependent on the PG due to the

presence of pumps and electric valves. The functionality of all the considered physical networks affects the STN response (e.g. emergency rescue and evacuation, human behavior).

3. MODELING THE BUILDING PORTFOLIO

Performing urban large-scale simulations, some generalizations and simplifications on the building portfolio are necessary to overcome the lack of data and to limit the computational workflow. Therefore, a *surrogate* model to describe the lateral behavior of each building is herein adopted by considering the relationship between its base shear and top horizontal displacement (Marasco et al. (2017); Noori et al. (2017)). The lateral stiffness properties are modeled through a parameterized backbone curve, where the post-elastic line is characterized by progressive decreasing stiffness, while hysteresis is accounted through the Takeda model (Takeda et al., 1970).

3.1 Building exposure database

An essential advantage of the *surrogate* model is the limited computational effort it requires with respect to a more refined finite element model, providing a significant benefit for large-scale urban simulations. However, it presents several practical challenges because detailed information about each building is generally not available. To overcome this issue, different methods have been proposed to classify the building stock based on their typical characteristics (Crowley et al., 2013; Lu & Guan, 2017). Although rapid, these methods are not so accurate because they could give similar results for buildings with different structural characteristics.

The approach proposed herein can collect data from different public and accessible sources. Based on the building stock of the city of Turin, general geometrical parameters (e.g., footprint area and total height) have been obtained from OpenStreetMap (Haklay & Weber, 2008), while

more detailed information (e.g., number of stories, year of construction) have been found in Geographical Information Systems (Maguire, 1991). Besides, further public information (provided by Municipality or other authorities), census data (provided by National or regional Statistical Institute, ISTAT (2016)), and other technical information (e.g. real estate data, design guidance) have been exploited to increase the level of knowledge.

Data analysis has been performed to identify common patterns; e.g. building's age has been correlated with the adopted design methods and parameters (e.g. load combinations and material strength classes), which has been used to estimate the minimum required geometrical and mechanical characteristics of the structural components. However, this procedure may lead to discrepancies with real data. Therefore, uncertainties characterization has been introduced to face the statistical nature of data, considering the buildings' parameters as normally distributed Random Variables (RVs).

Correlation among the different variables used in the analysis may also exist. In this study, the correlation between the reinforcement percentage and the characteristic reinforcing bar yield strength has been considered according to the Probabilistic Model Code (Vrouwenvelder & Faber, 2001). Also, a correlation between characteristic compressive strength and the elastic modulus of the concrete (Mirza & MacGregor, 1979) has been considered assuming a correlation coefficient of 0.8.

The flowchart of the data analysis is shown in Figure 2. Sources are illustrated on the top of the scheme as they contribute to the data collection phase. Then, correlations among the variables are considered in the data processing phase, and, finally, the processed data are stored in a standard format to create a comprehensive building exposure database.

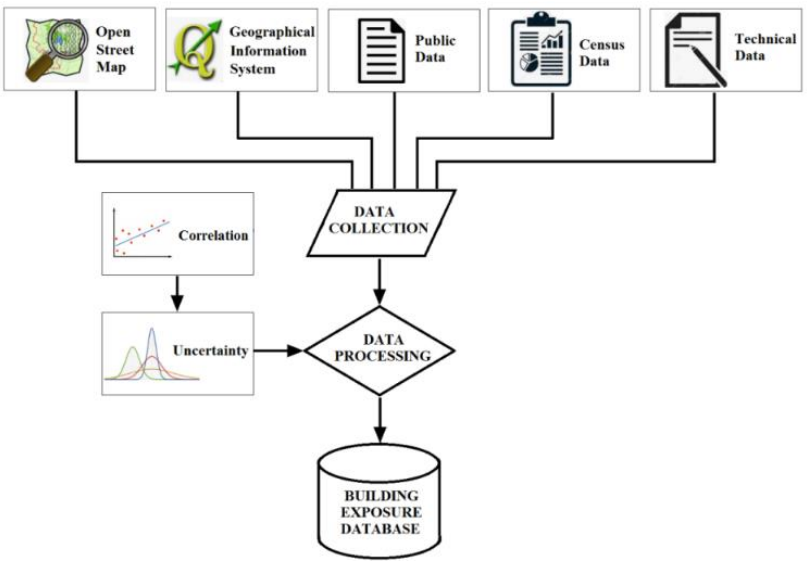

Figure 2. Flowchart of data analysis.

3.2 Backbone curve estimation

Each building is modeled as Multi-Degree-Of-Freedom (MDOF), which is subjected to a monotonically increasing lateral force distribution proportional to its fundamental mode. Elastic parameters are identified by the values of base shear and top displacement that cause the yield of the weakest column. Post-elastic parameters are assessed based on the upper-bound theorem of limit analysis and the equal energy rule (Marasco et al., 2017). These parameters allow to define a backbone curve representative of an equivalent Single-Degree-Of-Freedom (SDOF) model for each building. Four-point and three-point parametrized backbone curves are adopted for RC and masonry buildings, respectively.

All building's parameters that are significant to predicting the global structural capacity are assumed lognormally distributed RVs. Each statistical distribution is represented by the median (μ) and dispersion value (σ). The latter is based on the completeness of the quality and confidence associated with the building parameter that depends on its level of knowledge. In

the proposed methodology, three classes of building parameters are identified that are: mechanical-based (*M*), geometrical-based (*G*), and construction-based (*C*). For each class, a certain standard deviation has been set based on the building archetype and year of construction (Table 1).

Table 1. Standard deviations associated with the mechanical, geometrical, and construction-based parameters for RC and masonry buildings based on the year of construction.

		Year of construction					
		< 1916	**1916-1937**	**1938-1974**	**1975-1996**	**1996-2008**	**> 2008**
RC	σ_G / μ_G	0.20	0.18	0.16	0.13	0.1	0.08
	σ_C / μ_C	0.25	0.22	0.20	0.18	0.15	0.10
	σ_M / μ_M			0.20			
Masonry	σ_G / μ_G	0.25	0.22	0.2	0.17	0.13	0.10
	σ_C / μ_C	0.28	0.26	0.24	0.22	0.20	0.18
	σ_M / μ_M			0.25			

The standard deviation values are higher for old buildings since some of the building information lack of precision. Furthermore, a larger standard deviation is found for masonry buildings. The mechanical parameters refer to the compressive and tensile strength and elastic modulus of the constitute materials (concrete, bricks, stones, steel rebar), while the geometrical parameters are represented by the dimensions of the structural components (e.g. span length, cross-section width and depth, percentage of reinforcement). Finally, the construction-based parameters comprise all those variables that affect the building design such as the vertical and horizontal loads and the type of deck and external walls. The building data collection has been discussed in detail in the previous section.

The backbone curve is computed for each single building by varying its parameter through Monte Carlo Simulation (MCS) in the range $\mu \pm \sigma$. The iterative process ends when the output

dataset is consistent and provides a stable estimate of the median backbone curve which represents the global building's capacity. As 7-story RC and 4-story masonry buildings built in 1930 and 1978, respectively have been considered. The estimated median backbone curve for the RC and masonry buildings have been illustrated in Figure 3.

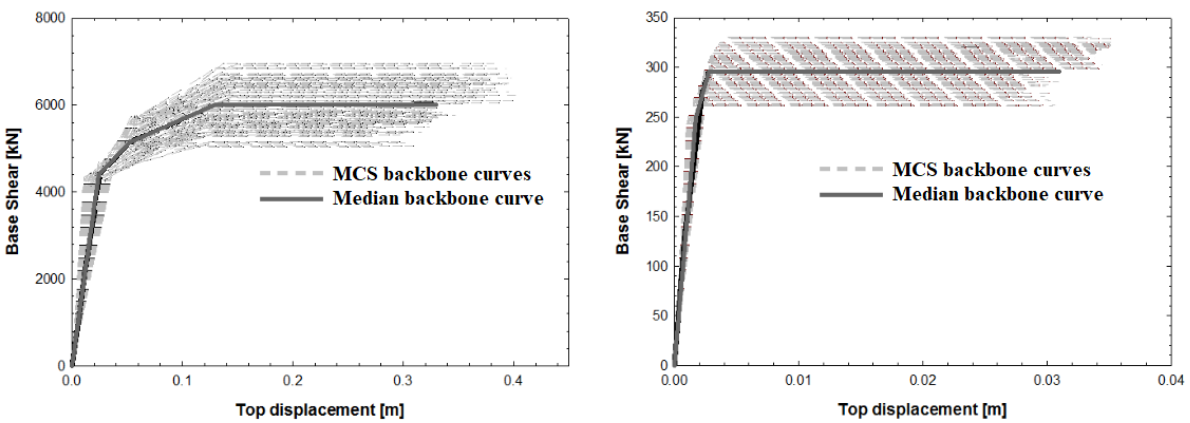

Figure 3. Backbone curves obtained through MCS and estimated median backbone curve for (a) RC and (b) masonry buildings.

3.3 Nonlinear time history analyses

Structural analyses have been carried out through the finite element code OpenSees (Mazzoni et al., 2006). Recent advances have been introduced by Zhu et al. (2018) to offer multi-interpreter capabilities resulting in the release of an "OpenSeesPy" library in Python. It has been used to implement the *surrogate* model and to perform the nonlinear time history analyses.

Each building has been modeled as "*ZeroLength*" element through two overlapped nodes. Initial stiffness and proportional damping corresponding to the median backbone curve are assigned to each element in both horizontal directions. Uniaxial "*MultiLinear*" material is employed to simulate the force deformation relationship, while the Takeda model is adopted

to consider the hysteresis. Seismic input consists of a pair of time histories (in both horizontal directions) applied at each element's location.

A simplified seismic scenario is assumed by defining epicenter location, moment magnitude, and time history recorded in the epicenter. Seismic inputs at any building locations are estimated based on Ambraseys' ground motion model (Ambraseys et al., 1996), while frequency changing is neglected. Therefore, nonlinear time history analyses are performed and the maximum top displacements of each element are computed.

3.4 Multiprocessing computation

Advancements in computer knowledge and architecture have led to the development of algorithms that can speed up the entire computational process through parallelization techniques. In parallel and distributed systems, Graphics Processing Unit (GPU) or Central Processing Unit (CPU) solvers can be adopted. GPU solvers exploit the high computation power of NVIDIA CUDA (Kirk, 2007) to significantly decrease the simulation time. Numerical GPU algorithms can be substantially accelerated as long as the algorithms map well to the specific hardware's features. For limited bandwidth problems that do not aim to the solution of a large complex matrix, the GPU solution might not be optimal because it causes poor or negative speedups (Ament et al., 2010). Thus, CPU-solvers may be adopted using parallel programming based on *threading* and *multiprocessing* processes. The first process consists of breaking the process within different parts while running the tasks that have access to the same memory areas. Instead, multiprocessing consists of submitting multiple processes independently to separate memory locations. The main advantage of multiprocessing is that it avoids conflicts in case the processors are assessing the same memory location at the same

time; therefore, it is appropriate for distributed memory systems with several CPU processors (e.g. supercomputers).

Given the considerations above, in the present study, the multiprocessing Python standard library has been used. The nonlinear time history analysis of each building has been assigned to different memory locations (Figure 4). A Rack Server with no. 2 Intel Xeon (E5-2698 v4 2.2GHz, 50MB Cache) and 256 GB RAM (8x32GB DDR4, 2400MHz) has been employed in this study. A schematic representation of the procedure used to speed up the processes is shown in Figure 4.

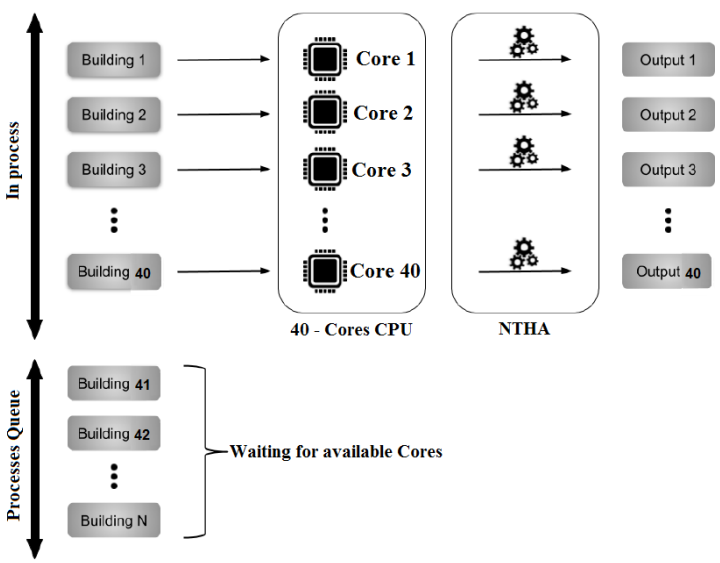

Figure 4. Multiprocessing scheme.

4. ROAD TRANSPORTATION NETWORK (RTN)

Road infrastructure connectivity within and among communities is essential to provide services and to forward social and economic growth. This topic has inspired several studies that developed different tools to investigate properties of large-scale transportation networks, from Python packages like NetworkX (Hagberg et al., 2008) to open source software such as Gephi (Bastian et al., 2009). Graph theory principles are certainly one of the most frequent tools in this field due to their simplicity and effectiveness to solve problems related to routing, traffic, minimum cost flow, etc.

Ideal City's road transportation network (RTN) has been modeled as an undirected graph *G* (each path can be passed through in both directions) that consists of 14,239 nodes (*N*), representing the road's intersections, and 18,798 edges (*E*), i.e. the links. Despite road maps are directed graphs, as streets have a certain directionality, the choice of modeling the system as an undirected graph has been followed because, in emergency conditions, directionality is not respected to give priority to evacuation and rescue operations.

Theoretically, the network has been described with an $N \times N$ adjacency matrix *A*. The elements inside *A* can be either 1 or 0. If $a_{i,j} = 1$, it means that node *i* and node *j* are connected, while $a_{i,j} = 0$ means that nodes *i* and *j* are disconnected. Since the graph is not directed, the resulting adjacency matrix is symmetric. The adjacency matrix allows computing many network parameters and quickly modifying the topology of the network, e.g. when roads are unavailable. An important global metric of graphs is the *average vertex degree* ($\langle vd \rangle$), which indicates how many edges cross a given node (Equation (1)).

$$\langle vd \rangle = \frac{1}{N} \sum_{i \in N} \sum_{j \in N} a_{ij} \quad (1)$$

In the case of an undirected graph, edges crossing a node should be considered only once, thus the adjacency matrix becomes triangular.

Global efficiency is another measure of network performance that was introduced by Latora and Marchiori (2001). It is defined as the average of the number of edges $d_{(i,j)}$ in the shortest path between nodes *i* and *j* (Equation (2)):

$$E_{glob} = \frac{1}{N(N-1)/2} \cdot \sum_{i \neq j} \frac{1}{d_{(i,j)}} \tag{2}$$

The plan view of the RTN with its main properties is shown in Figure 5.

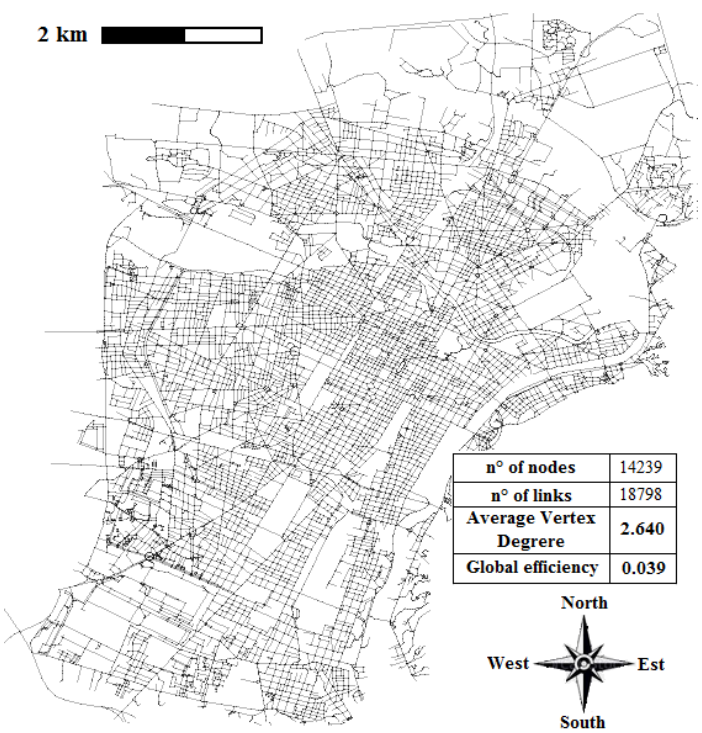

Figure 5. *Ideal City*'s RTN plan view.

4.1 Interdependency between buildings and RTN

The interdependency between buildings and the RTN following an earthquake is caused by the amount of the debris generated from the buildings' damage. To assess the amount of

generated debris, pictures collections by reconnaissance groups in the aftermath of worldwide seismic events have been used. These collections belong to publicly available databases: the Earthquake Engineering Research Institute clearinghouse and collection of case studies (EERI), the Geotechnical Extreme Events Reconnaissance (GEER), and the Digital Environment for Enabling Data-Driven Science (DEEDS) ones. Despite that these valuable sources contain thousands of images, only a small percentage clearly shows the amount of generated debris that can be measured. So after visual inspection, a database of 195 pictures has been selected.

Each selected picture shows a building suffering a partial or complete collapse after a seismic event. In total, 14 different earthquakes on different world regions have been considered, i.e., Central Italy (38 pictures), Cephalonia (6 pictures), South Napa Valley (6 pictures), Christchurch (9 pictures), Ecuador (32 pictures), Nepal (38 pictures), India (6 pictures), Loma Prieta (5 pictures), Central Mexico (20 pictures), North Iran (1 picture), Northridge (2 pictures), Armenia (5 pictures), Taiwan (26 pictures), Turkey (1 picture).

In the first step, the following information has been collected: (i) the earthquake magnitude, (ii) the epicentral distance, and (iii) the year of construction, (iv) the building archetype, (v) the building height and (vi) the number of stories. Then, each picture has been visually inspected to identify objects, such as vehicles, whose dimensions can be estimated. Starting from these reference measures, the extension of the debris with acceptable accuracy has been evaluated (Figure 6). Let P be the dimension of a reference object and p the debris' extension measured in pixel (px). Let D and d be the corresponding measures in m of the reference object and the debris extension, respectively. The debris extension d can be computed using

Equation (3).

$$d = p \cdot \frac{D}{P} \tag{3}$$

Then d is normalized by the building height to reduce its variance, allowing an easier comparison across different models.

Figure 6. Example of debris extension evaluation.

Then, two machine learning (ML) algorithms have been considered: Random Forest (RF), and k-Nearest Neighbors (KNR) algorithm (Liaw and Wiener (2002), Piegl and Tiller (2002)). The KNR algorithm predicts a new data point starting from the closest data in the training datasets, i.e. its "nearest neighbors" (Ni & Nguyen, 2009). Where 'k' stands for how many samples are used to evaluate the prediction. An RF, instead, is essentially a collection of randomized decision trees (Yao et al., 2011). The idea behind RFs is that multiple trees might reduce the problem of overfitting with respect to a single decision tree. There are two ways in which the trees in a random forest are randomized: by selecting the data points used to build a tree and by selecting the features in each split test.

Both selected algorithms have been tuned to obtain the optimal result and accuracy. In the KNR algorithm, the tuned parameter is the number of neighbors taken into consideration to evaluate the predictions in a χ test. This parameter k has been set equal to 5. Instead in RF, three parameters have been tuned: (i) the maximum depth of the tree (set to 10), (ii) the number of trees in the forest (set to 20), (iii) the minimum number of samples required to split an internal node (set to 40).

The two algorithms have been used to estimate the extension of debris and they have been compared using the R-squared and the mean absolute relative distance (MARD).

The R-squared measure provides a measure of how well future samples are likely to be predicted by the model by evaluating how much the scatter points are distant from the regression fit line calculated by the algorithm. R-squared measure ranges from 0 to 1, where 1 means perfect matching. MARD is the average vertical distance between each point and the regression line. Therefore, the lower the value of MARD and the more accurate the predictions.

Results from the training of the algorithms show that KNR algorithm gives a better MARD score (0.32), but a lower value of R-squared (0.42) with respect to RF, which means that more data are needed for KNR. Instead, RF gives better results both in terms of R-squared (0.52) and MARD (0.22) and therefore this algorithm has been selected and implemented in the platform.

5. POWER GRID

Urban PGs consist of a transmission system, which runs for long distances at high voltages, and a distribution system, which delivers electricity at medium and low voltage. The low

voltage line (i.e. 230 V single-phase, 400 V three-phase for European countries) supplies domestic and small commercial customers. Usually, at the city-level, PGs follow the main streets and may run both overhead and underground.

Various methodologies are available in the literature to assess the seismic damage to the electric infrastructure (Cavalieri, Franchin, Buriticá Cortés, et al., 2014). However, they require a large amount of data about the network's components, which is often not shared by stakeholders and public authorities.

Moreover, most of these methods assess the resilience of power distribution networks adopting the inherent fragility of the electrical components. However, in most cases, electrical components can withstand seismic excitation, while the buildings where they are installed are subject to serious seismic damages. The debris generated from partial or complete collapses damages electrical components, compromising the functionality of the entire PG. The weakest element of PGs are often distribution substations as discussed in Fujisaki et al. (2014). Fragility of substations varies whether their components are anchored or unanchored. Cavalieri, Franchin, and Pinto (2014) reported a complete overview of the main recent works on fragility functions of electric power system components, with the indication of the methodology used to evaluate the curves, the components considered and the damage states and indices. Considering the HAZUS methodology (Agency, 2003), to have extensive level of damage (i.e., repairs needed to restore functionality), the median peak ground acceleration (PGA) should reach 0.34g for low voltage substations with unanchored components and 0.45g in case of anchored components. These values of PGAs are most likely to cause serious building damage given the typical built environment of European cities. Therefore, in this paper, the

vulnerability of the PG is related to the damage occurring to the buildings where substations are located. In other words, if the building where a substation is installed collapses, the grid components in that substation fail. Consequently, when a substation fails the electric load drops to zero, and all the buildings connected to that substation are without power.

The fragility of distribution lines has not been considered since at the urban level distribution lines are more robust than distribution substations. Distribution lines can run both overhead and underground, despite modern cities prefer to let the system run underground as it is safer and more efficient. In Ideal City, they are mainly meant to be underground. Generally, failure of underground lines happens only in case of strong shakes with significantly large ground deformations, which would cause serious building damage anyway. On the other hand, overhead distribution lines are mostly affected by strong winds, while their vulnerability to earthquakes is limited due to the small size and slenderness of urban utility poles.

Ideal City's PG consists of 15 primary substations and 1274 distribution substations (Figure 7). The primary substations operate at high and medium voltages and are supposed to be

located in robust facilities so that they can keep operating even after strong ground motions.

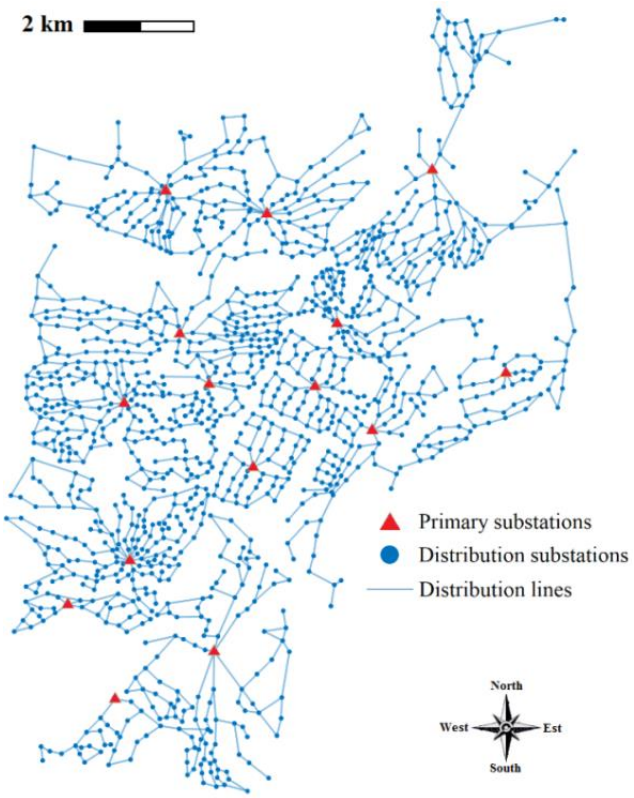

Figure 7. *Ideal City*'s PG.

5.1 Interdependency between buildings and PG

The power system of *Ideal City* has been modeled following the *Density Design Method* (DDM) proposed by Cardoni et al. (2019). The DDM is based on the idea that the fragility of electric substations is the same as the buildings hosting them. Therefore, the electric components and the buildings where they are located are assumed as a series system with their corresponding fragility functions, so the weakest component limits the overall system reliability. This approach allows to implicitly take into account the interdependency between the power network and the building portfolio. The DDM allows for a detailed analysis of the

system, as the PG is specifically designed instead of using an existing database. Thus, population density, power load density, and system properties (e.g., feeders' length, load types, buses' redundancy, etc.) are the main design parameters. The first step consists in dividing the area covered by *Ideal City* into districts to locate primary substations. These are characterized by a medium voltage (MV) scheme of 22 kV. Then, electrical loads are identified following the procedure described by the 2016 European guidelines (Prettico et al., 2016). Based on the area and population of each district, the design load is estimated. In detail, the adopted design load density is assumed to be 8 MVA/km^2 for each district. This information is needed to identify the distribution substations containing transformers. Transformers can be of three types, i.e., 0.40 MVA, 0.63 MVA, and 1.00 MVA. The chosen distribution is 60%, 30%, and 10% respectively, in accordance with current best practices. Overall, Ideal City's PG consists of 1,274 distribution substations. Table 2 summarizes the number of distribution substations for each power category.

Table 2. Ideal City's distribution substations.

Distribution substation type	**Total number**
0.40 MVA	766
0.63 MVA	382
1.00 MVA	126

Distribution substations are evenly located in the district considering power demand so that each of them supplies a different number of buildings. Substations located in buildings that are extensively damaged or collapsed after an earthquake are assumed to fail. Besides, since the distribution substations are connected in series, once a substation fails all the downstream

substations will also be unfunctional. Consequently, the number of buildings and users not supplied after the seismic event can be determined.

6. WATER DISTRIBUTION NETWORK (WDN)

The WDN serviceability implies enough water supply to fulfill the demand and reasonable water pressure. The damages induced by seismic events are likely to cause a drop in the water pressure and consequently a limited water supply.

In this research, urban water consumption is extrapolated from national census data and the layout of the WDN of *Ideal City* has been assumed to overlap the RTN. Elevations of WDN's nodes have been gathered from Google Maps (Svennerberg, 2010). Collected data have been processed through the Water Network Tool for Resilience, which is a Python package designed to simulate and analyze the resilience of water distribution networks. This tool allows controlling EPANET 2.0 (Rossman, 2000) using Python.

The water demand at each node (junction) depends on the number of people served by that node. The number of the population served by each node has been estimated from the number of households around that node.

Water distribution systems consist of interconnected components including primary and secondary pipelines, storage facilities, and components that convey water on buildings based on the closest distance between the primary pipeline and the buildings inside the mesh (Figure 8a).

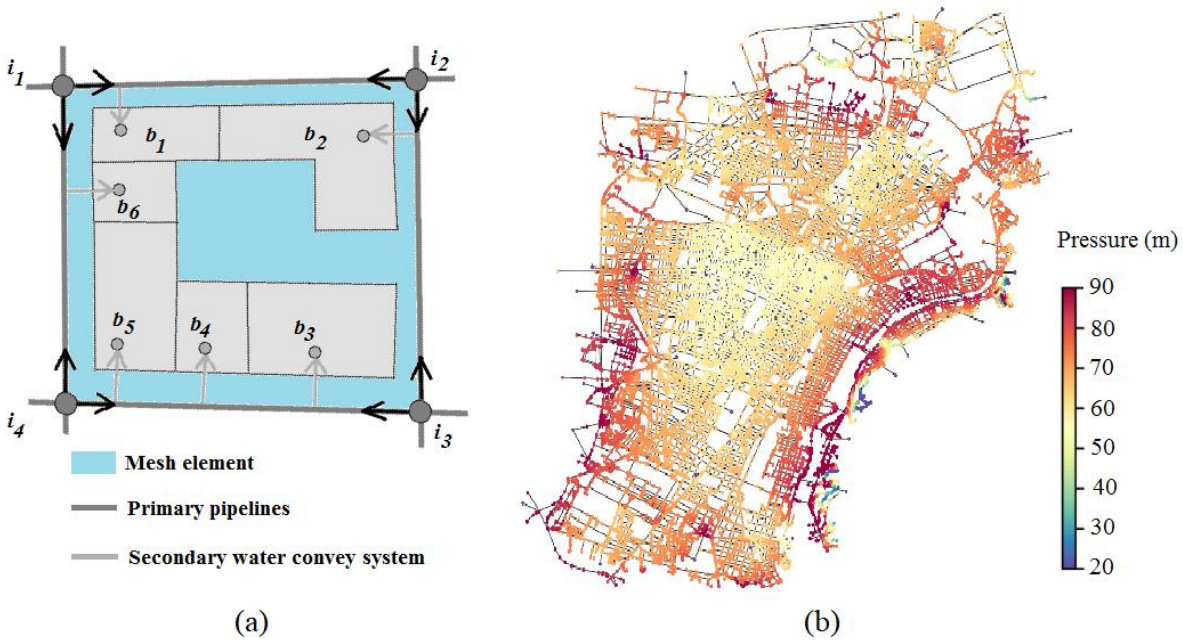

Figure 8. (a) Water demand in w^{th} element, i^{th} nodes of the element, and water convey on buildings within the element. (b) Water pressure of the WDN after calibration.

The calibration of a WDN of such a size brings on several difficulties. It is a fundamental issue to ensure an accurate and realistic simulation for both the flow velocity and pressure. The pipes diameters and the positions of the valves, pumps, reservoirs, and tanks have been determined to ensure the following constraints (Equations (4),(5)):

$$0.5m/s \leq \text{Velocity} \leq 2m/s \tag{4}$$

$$40m \leq \text{Pressure} \leq 80m \tag{5}$$

Figure 8b shows the calibrated WDN at the peak hour of water demand. More details about the network's generation methods and technical criteria can be found in (Taurino et al., 2018).

6.1 Vulnerability of the WDN

The reliability of a water network is connected to the concept of vulnerability of its elements. Herein, the focus is given to the pipe because it is the most challenging component to inspect and replace, and also its extensive distribution and exposure make it especially vulnerable. In this work, the seismic vulnerability of the buried pipelines introduced in the American Lifelines Alliance (Eidinger et al., 2001) is adopted.

The seismic wave propagation induces strains to the pipes due to the soil-pipe interaction. Strains could produce damage if the pipe strength is exceeded. When pipe damage occurs, the pipe is assumed to break in the middle. In the context of this work, only major damage is assumed to cause water leakage. Pipe damage is modeled dividing the pipe into two equal parts. Then two reservoirs are added at their endpoints to simulate the water leakage through the crack. The reservoirs have a total head equal to the elevation of the middle point of the pipe (assuming that the pipe breaks in the middle). A check valve is inserted so that water only flows towards the reservoirs.

A combined demand-driven and pressure-driven analysis is conducted to account for the dependence of water supply on pressure. First, a Demand-driven analysis is performed; then, nodes with pressure below the value required to satisfy the demand are converted into Emitter nodes.

6.2 Interdependency between buildings and WDN

Once a seismic event occurs, an additional drop of pressures might be considered due to the damage to the secondary water system. In this study, a further drop of pressure in the pipelines system is considered when “extensive” or “complete” damage occurs in a household located

within the closed-shaped WDN. In other words, the building damage scenario is used to update the water supply of the WDN.

6.3 Interdependency between PG and WDN

The functionality of WDN is dependent on the power system due to the presence of pumps and electric valves. In the aftermath of a seismic event, a power outage may occur leading to a temporary inoperability of the electric device of the WDN. In this study, the interdependency between PG and WDN is taken into account by identifying the unpowered pumps and then updating the EPANET model accordingly. A new state of nodal pressure and water supply is then generated.

7. EMERGENCY EVACUATION MODELLING

The implemented platform includes STN that consist of an agent-based model (ABM), which can manage 900,000 individual agents that dynamically interact with each other and with the urban scenario. Furthermore, the ABM can be used to model other objects, such as shelters, hospitals, and ambulances that are governed by different rules. Therefore, an emergency evacuation can be simulated, and specific emergency plans can be designed to study and improve the community response.

The ABM layer is also able to manage the interdependency between the agents and the other layers (i.e. the built environment, the generated debris, and the road network). Furthermore, the evacuees have been implemented with individual characteristics including human behavior and considering different levels of agent health obtained from the seismic damage simulation. Figure 9 reports evacuating agents, where the level of injury severity is associated with the

agent color (e.g. green normal conditions, orange slight injured), and the evacuation velocity depends on the injury level.

Figure 9. Simulation of an evacuation procedure using virtual reality. The color of each agent indicates her health conditions.

The ABM environment has been developed in Unity (UnityTechnologies, 2020). The input data needed to develop the ABM scenario are collected from the other infrastructure layers implemented in the platform. Indeed, the data collected are: (i) the estimated post-disaster building damage that reflects in (ii) number of injuries and (iii) road blockage due to debris.

7.1 First aid modeling

The ABM STN layer considers two classes of agents, the individuals, and the ambulances; the last ones pick up severely injured individuals and transport them to hospitals. On the contrary, lightly injured agents preserve their walking capabilities and reach hospitals on their own (Figure 10). Healthy agents can remain close to their buildings or walk to the nearest emergency shelter accordingly to a random procedure that is parameterized as a function of damage level suffered by the buildings.

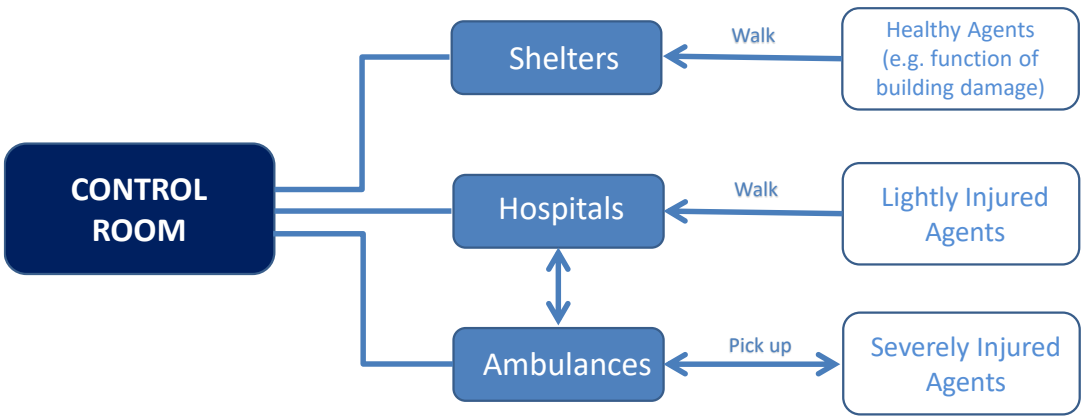

Figure 10. First-aid organization in the ABM layer.

Shelters have a fixed capacity, beyond which the individual starts walking toward the closest town exit. Also, hospitals have a fixed capacity, except for those that can deploy a field hospital. In this case, an infinite capacity is assumed to guarantee assistance to all injured individuals. A control room manages the hospitals and shelters monitoring the available information and making decisions about resources. The buildings may contain a number of individuals and contain a variable number of individuals function of the time of the day.

7.2 Modeling human behavior and emotions in ABM

During the emergency evacuation, two frequent individual phenomena can be recognized: the leader-follower and the emotional (e.g. altruism, panic) behavior. The first one is recognized as the static and predictable component because it remains unchanged throughout the process. Instead, the second one, the dynamic component, is generally unpredictable because characterized by emotions. It can be modeled using the Belief-Desire-Intention (BDI) model and implemented through a matrix approach by the Extended Decision Field Theory (EDFT) to cope with the dynamically changing environment (G. P. Cimellaro et al. (2019), G. P. Cimellaro et al. (2017)). It presents a dynamic and probabilistic mathematical approach to

reproduce the individual decision-making process in the changing environment. It is summarized by the following relation that allows to compute the preferences P among m options expressed by an agent durint the simulation time (Equation (6)).

$$P(t+h) = SP(t) + CM(t+h) \cdot W(t+h) \quad (6)$$

where $P(t)^T = [P_1(t), P_2(t), ..., P_m(t)]$ are the preference in percentage and $P_i(t)$ is the strength of the preference corresponding to option i at time t. The first term is the product of the preference chosen at the previous state and the stability matrix S that provides the memory effect. The second term reproduces the emotional individual behavior in the changing environment, where M is the value matrix that represents the subjective evaluations (perceptions) of a decision-maker, W is the weight vector that allocates the weights of attention corresponding to each attribute of M, and C is the contrast matrix that compares the weighted evaluations of each option. Matrix C is the identity matrix if each option is evaluated independently (G. P. Cimellaro et al. (2019), G. P. Cimellaro et al. (2017)).

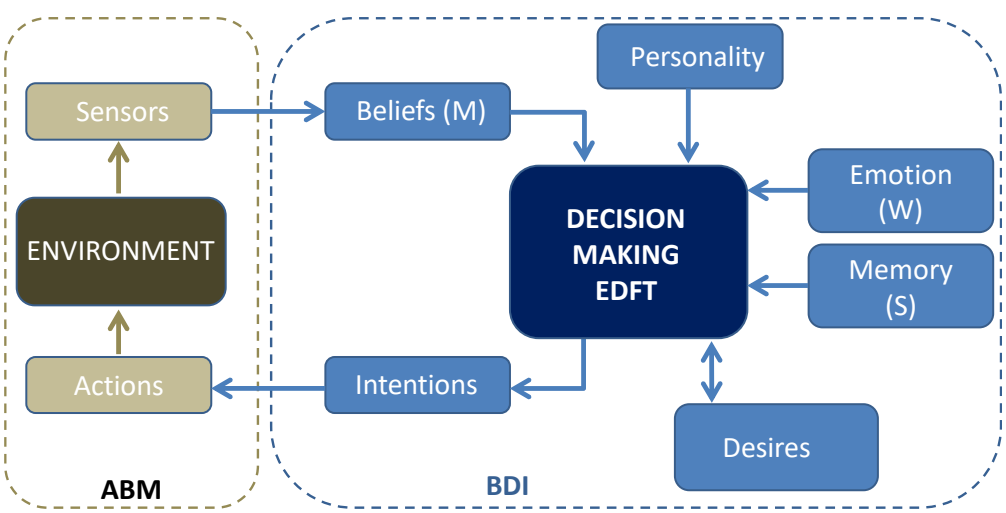

Figure 11. EDFT architecture and interaction of the human behavior modules (adapted from G. P. Cimellaro et al. (2019).

7.3 Interdependencies with other networks

The interdependency between the evacuees and the built environment consists of the debris generated by the earthquake-induced damages to buildings. As a cascading consequence of debris accumulation, the road network can be interrupted entailing an overall increase in the average number of people who have difficulty evacuating and an essential risk that some individuals cannot evacuate at all. Furthermore, the first aid network supported by ambulances that intervene in the recovery of seriously injured individuals can be unable to access those parts of the urban system most affected by damage to buildings and debris.

The debris generation is also included in the ABM layer with the approach already detailed in Section 4.1. Thus, the hybrid characteristics of *Ideal City* allow both the estimation of buildings' damage and debris' generation and the analysis of their cascading effects. In detail, individuals could be killed, injured, or trapped inside damaged buildings or *Ideal City* portions. Moreover, the transportation network can be interrupted blocking the ambulances' intervention and affecting the escape routes for evacuees.

8. APPLICATION

The objective of this work is the development of an integrated platform to assess seismic resilience at the community level for large-scale areas. Five layers have been considered to model community infrastructures, while different physical methods have been implemented to evaluate the infrastructures' vulnerability and their mutual interdependencies. The flowchart

depicted in Figure 12 provides a detailed description of the methods and processes used in the platform.

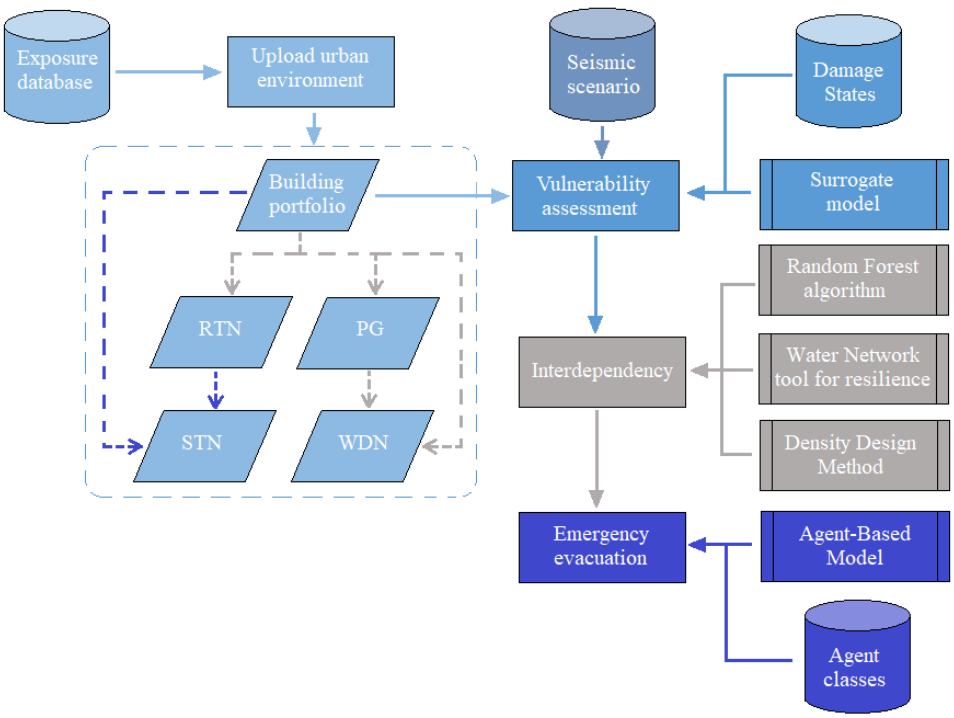

Figure 12. Flowchart of the integrated platform.

All the inherent data of the infrastructures are stored in the exposure database. Building stock represents the main physical layer whose vulnerability is assessed by using a *surrogate* model based on certain damage states and seismic scenario. The platform allows users to upload exposure database, while selecting the damage states and the related Engineering Demand Parameters. Ghobarah (2004) damage states and related maximum inter-story drift thresholds are set by default in the integrated platform. The user can also define the seismic scenario by selecting (*i*) epicenter location, (*ii*) magnitude of the earthquake, (*iii*) time-history recorded at the epicenter, and (iv) ground motion prediction equation to evaluate the geometrical attenuation at any building location. Ambraseys et al. (1996) attenuation model is set by default

while seismic record processing is performed by the embedded OpenSignal tool (Cimellaro & Marasco, 2015).

The simulated damage experienced by the buildings is the starting point for taking into account the cascading effects on the RTN, PG, and WDN. Interdependency between buildings and roads is accounted through an RF algorithm which provides the functionality state of each roadway element. Furthermore, the Density Design Method is applied to PG by setting off the transformers located within irreversibly damaged buildings. Based on the buildings' damage and PG's unfunctionality, the Water Network tool for resilience is employed to evaluate the effects on the WDN. Under these conditions, the emergency evacuation is simulated through an Agent-Based model after fixing the common rules adopted by the agents.

An application of the developed platform to *Ideal City* hybrid model is herein presented. The virtual city consists of 23420 residential buildings and covers an overall area of 120 km^2 with a population of 908.129 inhabitants. The building stock of the city is mainly composed of RC buildings (63%) and masonry structures for the remaining parts (37%). Figure 13 illustrates a screenshot of the software's graphical user interface and the related analysis options.

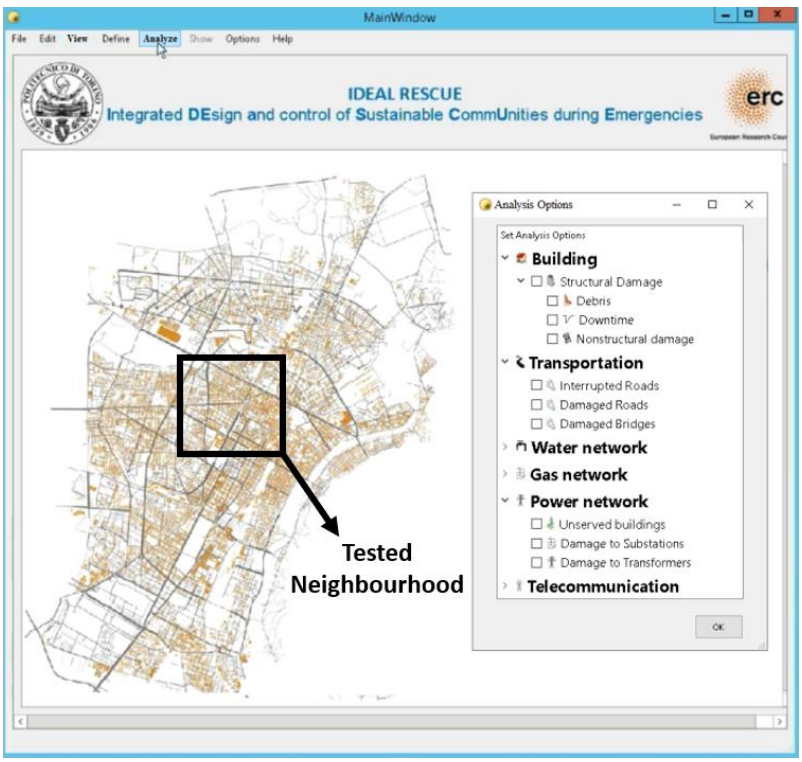

Figure 13. View of *Ideal City* within the software's main window and the dataflow for a disaster simulation.

Different seismic scenarios have been adopted by defining the epicenter location, the moment magnitude, and the time history recorded at the epicenter. Geometrical attenuation at any building location has been estimated based on Ambrayses' attenuation Ground Motion Prediction Equation (GMPE) (Ambraseys et al., 1996).

Four benchmark horizontal acceleration time histories have been selected using Opensignal software (Cimellaro & Marasco, 2015). Northridge (lmar County Hospital parking lot in Sylmar, California) and Kobe (Kobe Japanese Meteorological Agency station, Japan) records have been assumed to simulate the effects of near-field earthquakes. On the other hand, El Centro (Imperial Valley Irrigation District substation, California) and Hachinohe (Hachinohe

City, Japan) records have been considered as far-field seismic benchmark scenarios. Table 3 lists the main seismological characteristics of each selected record.

Table 3. Characteristics of the four selected benchmark time histories.

	El Centro	**Kobe**	**Hachinohe**	**Northridge**
Date	5/18/1940	1/17/1995	5/16/1968	1/17/1994
Event	Imperial Valley	Hyogoken Nanbu	Tokachi-oki	California
M_w	6.9	6.8	8.2	6.7
Depth [km]	16.00	17.60	26.00	11.30
PGA [g]	0.35	0.82	0.23	0.84

The developed platform can provide damage information associated with all the layers of the analyzed area. Furthermore, the dataflow can be completely managed by the user who can choose among different options (Figure 13). Analysis flow starts with the damage assessment on the building portfolio. Once a seismic scenario is defined, a pair of horizontal orthogonal acceleration time histories have been applied at each building location by considering the geometrical attenuation.

Figure 14 depicts the Damage States (DSs) map of the selected district under different seismic scenarios. Table 4 lists the percentage of building DSs: Northridge and Kobe scenarios mainly have caused almost complete damage (about 86% and 79% of buildings, respectively). Only a few buildings have been found functional (around 1% ranging between undamaged and slightly damaged for both scenarios). Besides, 40% of moderate damage and 27% of complete damage has been experienced by the El Centro earthquake, while extensive and slight damage

665 corresponds to 14% and 19%, respectively. Hachinohe earthquake is the less disruptive
666 scenario where most of the buildings remain functional, 52% of buildings are either undamaged
667 or slightly damaged, 37% are moderately damaged, while only 9% collapse.

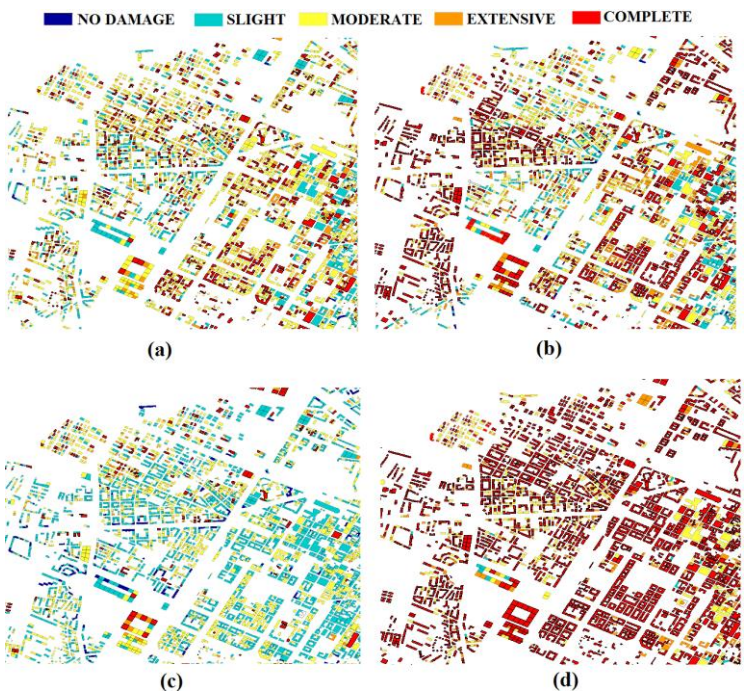

668

669 **Figure 14.** Building DS maps of *Ideal City* district for (a) El Centro, (b) Kobe, (c)
670 Hachinohe, and (d) Northridge earthquake scenarios.

671 Table 4. Percentage of buildings DSs for each scenario.

Damage States [%]	**El Centro**	**Kobe**	**Hachinohe**	**Northridge**
No damage	0.62	0.03	5.9	0.03
Slight	18.75	0.77	45.68	0.77
Moderate	39.38	9.53	36.73	7.17
Extensive	14.1	10.21	2.22	5.83

Complete	27.14	79.47	9.47	86.19

672

673 The possibility to use parallel computing to run this demanding computational analysis has
674 been investigated. First, Single Core (SC) and Multi-Core (MC) processing have been
675 compared in terms of elapsed time under different building cluster sizes. Figure 15 illustrates
676 the variability of the mean elapsed time ratio (speedup ratio) vs the number of buildings
677 involved during the analysis.

678 According to the numerical results, SC application is faster when the number of buildings is
679 lower than 10. This is because MC frameworks require more time for spawning processes,
680 assigning tasks, collecting data, and closing processes. Once the processes are spawned, they
681 can be used without closing processes. In the selected case study, the speedup ratio of MC
682 reaches the maximum efficiency when 1000 buildings are analyzed simultaneously. Under this
683 condition, MC is 36 times faster than SC. When the top performance is reached, then an
684 increase of the elapsed time is observed due to the thermal throttling caused by the CPU
685 overheating. Under this condition, the new speedup ratio is about 30 times faster than SC and
686 remains almost constant until the end of the analysis.

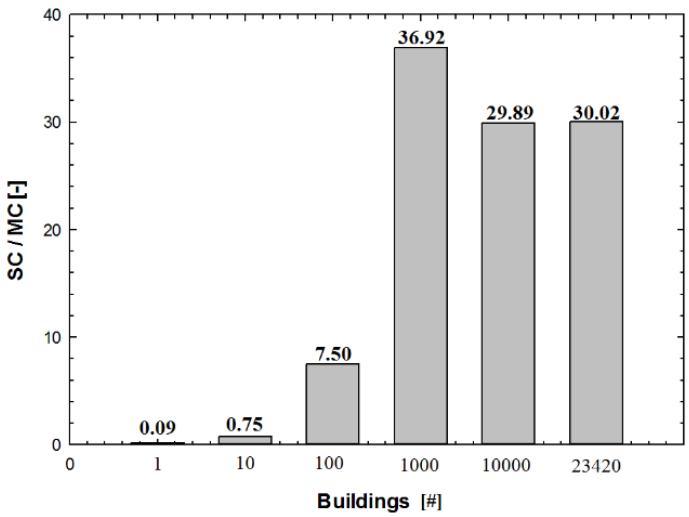

Figure 15. Speedup ratio between Single-Core (SC) and Multiprocessing (MC) computational process.

Once the building damage has been estimated, then different types of interdependencies have been investigated. First, the extension of debris caused by the building damage is evaluated using a machine learning algorithm and the corresponding obstructed roads are identified. Figure 16 illustrates the interrupted roads (red lines) caused by the four selected seismic scenarios for the considered district. Indeed, the Northridge earthquake has caused the largest number of blocked roads (30.48%) followed by Kobe (21.29%) and El Centro (14.49%), while Hachinohe is the less disruptive seismic event with only 4.47% of unfunctional roads.

The blocked roads are not equally distributed over the city. Indeed, some districts are completely isolated due to the amount of debris produced, highlighting the importance of this type of analysis to plan efficient evacuation and rescue operations. The *average vertex degree* and *global efficiency* have been calculated and normalized with respect to the undamaged conditions. Results are shown in Figure 17 where it is possible to see the two indices reducing with the increment of the earthquake severity.

703

704 **Figure 16.** Visualization of interrupted roads for (a) El Centro, (b) Kobe, (c) Hachinohe,

705 and (d) Northridge earthquake scenarios.

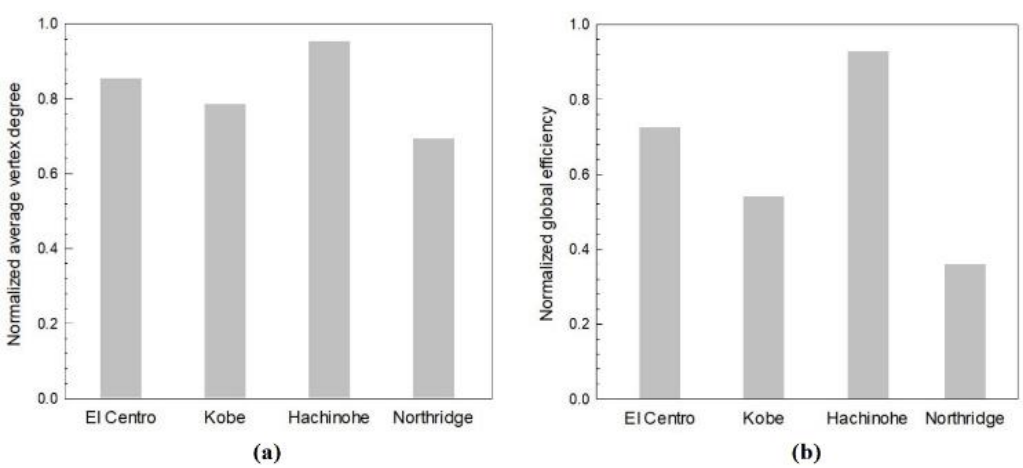

706

707 **Figure 17.** Variation of the normalized average vertex degree (a) and normalized global

708 efficiency (b) under different seismic scenarios.

The second interdependency that has been considered correlates the power distribution network with the building damage. The failed electrical substations for the four different seismic events are shown in Figure 18.

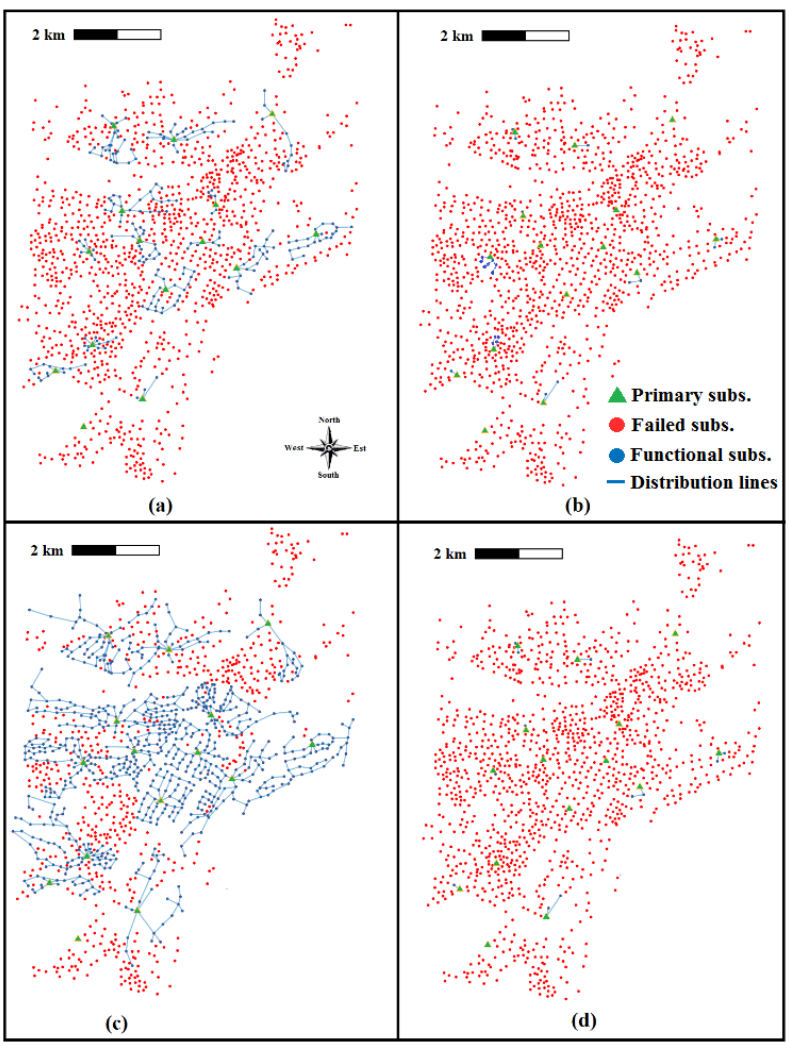

Figure 18. Visualization of PG failure's component for (a) El Centro, (b) Kobe, (c) Hachinohe, and (d) Northridge earthquake scenarios.

In detail, the substations that remain functional for Northridge are 12, for Kobe are 25, while for El Centro are 220, and for Hachinohe are 747 out of a total of 1274 substations. These results show that the near-field earthquakes are more disruptive than the far-field earthquakes

718 for the PG. In Figure 19 is shown the impact of the PG's disruption at the building level, where
719 in red are the buildings without power.

720 A simple resilience index (R_{power}) has been introduced as the ratio between the number of
721 users who still have access to electricity and the total population of *Ideal City*. 98.5% of the
722 population is without power after Northridge and Kobe scenarios, while about 80% of the
723 population has no power after the El Centro earthquake. Instead, Hachinohe causes a loss of
724 power for about 40% of users.

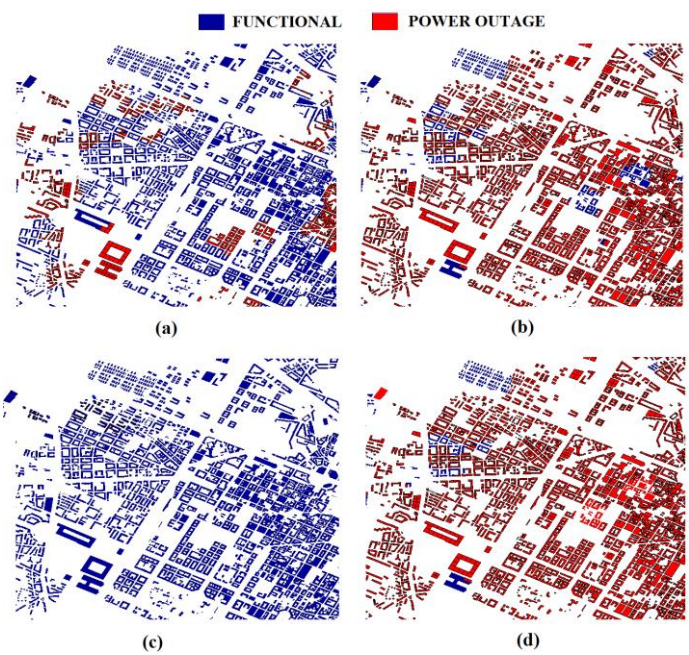

725

726 **Figure 19.** Visualization of buildings with and without electricity for (a) El Centro, (b)
727 Kobe, (c) Hachinohe, and (d) Northridge earthquake scenarios.

728 Finally, the damage caused by the four benchmark scenarios on the WDN has been
729 investigated. Northridge scenario induced the highest number of damaged pipes while
730 Hachinohe induced the lowest one.

Figure 20 depicts the drop in water pressure (*m*) in each building caused by the damage on the water pipes. The Northridge scenario induced the highest number of damaged pipes while Hachinohe induced the lowest one. The disruption of the pipes is a function of the earthquake characteristics, such as Magnitude, epicenter, depth, etc. Looking at Table 3 in the paper, Northridge earthquake, due to its shallow depth, is a near field earthquake. This makes it more disruptive for the water pipes of the *Ideal city*.

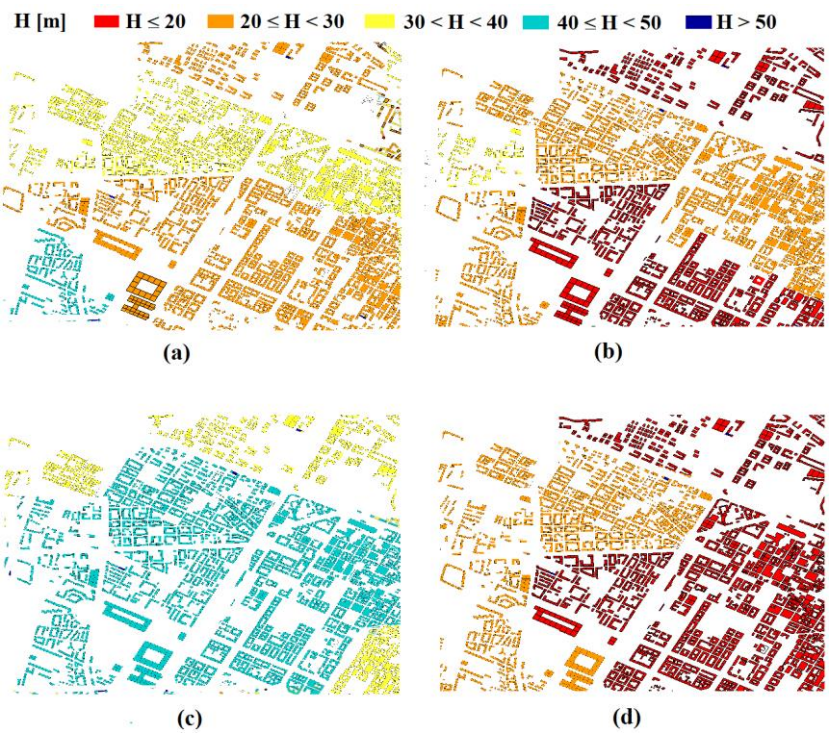

Figure 20. Water pressure distribution after (a) El Centro, (b) Kobe, (c) Hachinohe, and (d) Northridge earthquake scenarios.

Finally, the population response to emergency evacuation has been analyzed by the ABM layer of *Ideal City*. For example, the number of lightly injured individuals walking to hospitals and severely injured individuals that are waiting to be rescued are reported in Figure 21.

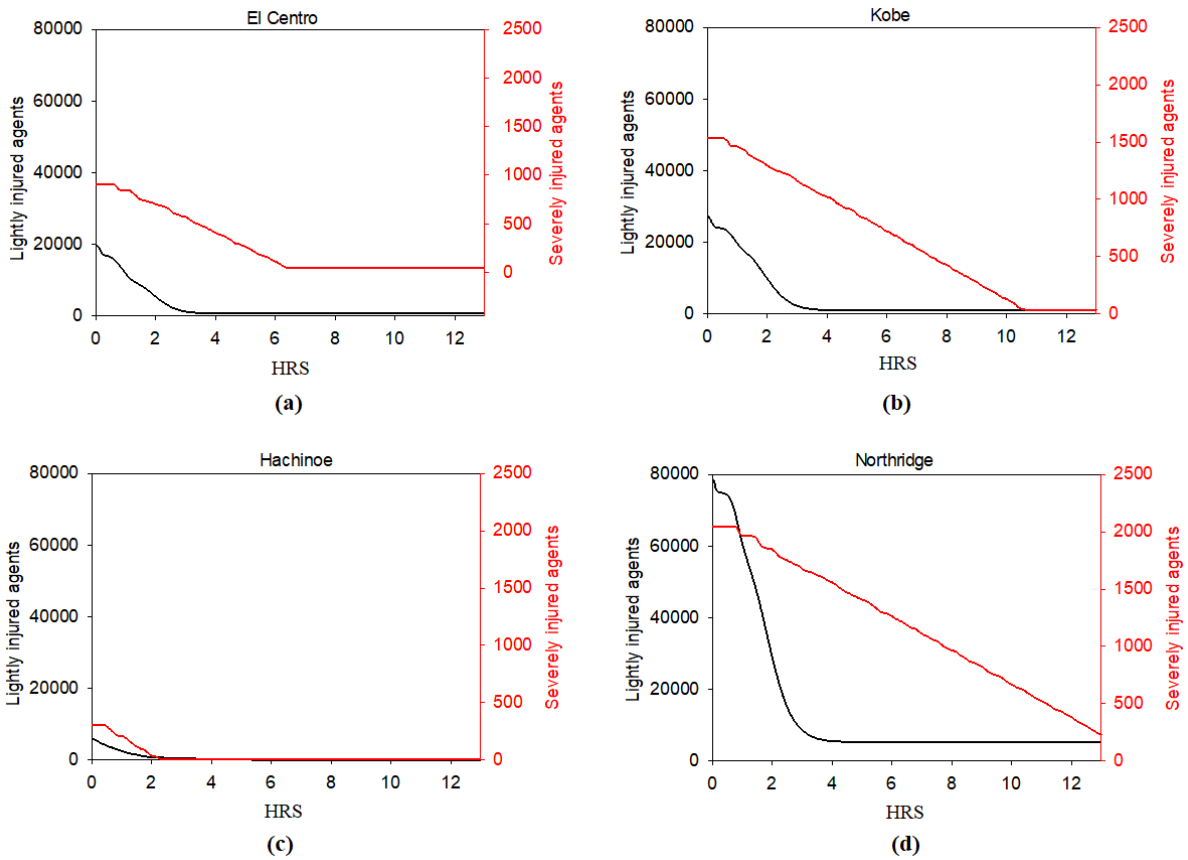

743

744 **Figure 21.** Lightly injured agents walking to hospitals and severely injured waiting to be
745 rescued vs time (hours): (a) El Centro, (b) Kobe, (c) Hachinohe, and (d) Northridge
746 earthquake scenarios.

747 Furthermore, the platform can also be adopted at the design stage, e.g. to compute the
748 minimum number of rescue resources (ambulances) to recover the seriously injured
749 individuals within a fixed period for a certain earthquake scenario (Figure 22).

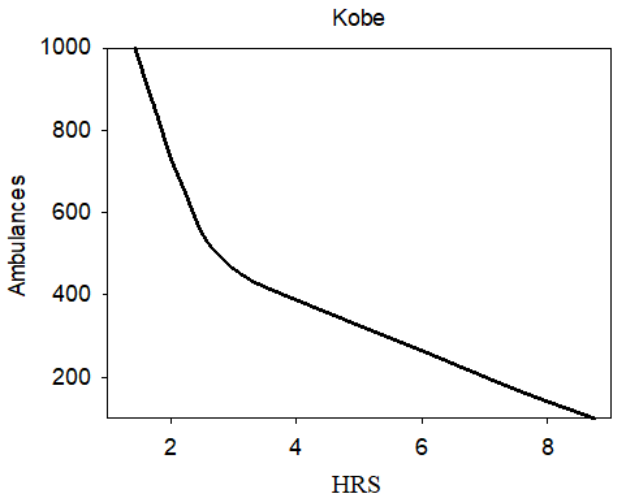

Figure 22. Kobe event: rescue time (hour of all severely injured individuals as a function of the number of ambulances.

The four seismic benchmark scenarios have caused similar effects for all the infrastructures within *Ideal city*. Northridge and Kobe have found to be more disruptive due to the higher PGA. These two near-field seismic scenarios have caused more than 90% of irreversible damage to the building portfolio. Their impact on the RTN have been also devastating, causing a considerable decrease in the normalized global efficiency of the transportation network around 45-55%. A similar trend has been found in the PG, where more than 98% is without power following the Northridge and Kobe earthquakes. Drastically reduction of water pressure has been also accounted for in the WDN after the occurrence of the two aforementioned seismic scenarios. Finally, the number of severely injured agents between 50000 and 60000 has been estimated.

The Hachinoe scenario has found as the less disruptive scenario for all the networks, while El Centro induced a considerable level of irreversible damage on the analyzed infrastructure. More than 40 % of building stock has experienced irreversible damage following the El Centro

scenario, while only 12 % has been found for Hachinoe. These results are also reflected on the RTN, where 75% and 40% of normalized global efficiency have been accounted. 20% and 60% of substations have been found functional following El Centro and Hachinoe scenarios, respectively. Finally, Hachinoe has caused only 10000 severely injured agents, while after the occurrence of El Centro scenario, more than 35000 severely injured agents have been found.

The large outcomes discrepancies between Hachinoe and El Centro are due to their seismological characteristics. Hachinoe is represented by a greater magnitude and hypocentral depth than El Centro. Therefore, the seismic wave propagation associated with the Hachinoe scenario is more affected by the geometrical attenuation. In fact, the PGA of Hachinoe is about 0.23g, while 0.35g is the one of El Centro. In the nonlinear time history analyses, such a kind of discrepancy of PGA will cause considerably different responses.

9. CONCLUDING REMARKS

A computational platform is presented in this paper to analyze the effects of seismic events on an urban community. The platform implements different layers, such as buildings, road transportation networks, power grid, water distribution networks, and socio-technical networks. Specific models have been developed to simulate the interdependency between different layers. The individual seismic response of each building is analyzed through a *surrogate* physical model, including inherent uncertainties. The seismic effects in terms of damage and serviceability for each layer can be computed and visualized. Furthermore, an agent-based model has been developed to simulate the emergency evacuation process and the first-aid operations in post-disaster conditions. Future work is geared towards including gas and telecommunication interdependencies in the analyses.

A hybrid model of a virtual city has been used to test the platform under four different seismic scenarios. The main innovative aspects and advantages of the proposed platform are: (i) damage and resilience assessment of critical infrastructures in a large-scale urban environment considering their interdependencies; (ii) graphic visualization of the results obtained by the different layers; (iii) multiprocessing computation; (iv) agent-based modeling for emergency management and evacuation.

The platform is intended to support decision-makers and planners to analyze the community response to a seismic event and implement possible countermeasures to improve the overall resilience. The long-term objective is to make individual infrastructures safer, implementing specific actions that allow each network to withstand external perturbations and to mitigate cascading effects due to interdependencies.

The current state of the platform does not allow considering the recovery of the damaged structure and infrastructure. This is actually a work in progress that will be included in a future paper. The future work will address both the damage and the restoration analysis of the infrastructure network by incorporation already-developed models within the platform (De Iuliis et al., 2019; Kammouh, Cimellaro, et al., 2018).

ACKNOWLEDGMENTS

The research leading to these results has received funding from the European Research Council under the Grant Agreement n° ERC_IDEal reSCUE_637842 of the project IDEAL RESCUE— Integrated DEsign and control of Sustainable CommUnities during Emergencies.

REFERENCES

Agency, F. E. M. (2003). Hazus MR4 Multi-Hazard Loss Estimation Methodology.
Alsubaie, A., Alutaibi, K., & Martí, J. (2015). *Resilience assessment of interdependent critical infrastructure.* Paper presented at the International Conference on Critical Information Infrastructures Security.
Ambraseys, N. N., Simpson, K. u., & Bommer, J. J. (1996). Prediction of horizontal response spectra in Europe. *Earthquake Engineering & Structural Dynamics, 25*(4), 371-400.
Ament, M., Knittel, G., Weiskopf, D., & Strasser, W. (2010). *A parallel preconditioned conjugate gradient solver for the poisson problem on a multi-gpu platform.* Paper presented at the 2010 18th Euromicro Conference on Parallel, Distributed and Network-based Processing.
Balaei, B., Wilkinson, S., Potangaroa, R., & McFarlane, P. (2020). Investigating the technical dimension of water supply resilience to disasters. *Sustainable Cities and Society, 56*, 102077.
Bastian, M., Heymann, S., & Jacomy, M. (2009). *Gephi: an open source software for exploring and manipulating networks.* Paper presented at the Third international AAAI conference on weblogs and social media.
Borgdorff, J., Krishna, H., & Lees, M. H. (2015). Sim-city: An e-science framework for urban assisted decision support. *Procedia Computer Science, 51*, 2327-2336.
Cardoni, A., Cimellaro, G., Domaneschi, M., Sordo, S., & Mazza, A. (2019). Modeling the interdependency between buildings and the electrical distribution system for seismic resilience assessment. *International Journal of Disaster Risk Reduction*, 101315.
Cash, D., Adger, W. N., Berkes, F., Garden, P., Lebel, L., Olsson, P., . . . Young, O. (2006). Scale and cross-scale dynamics: governance and information in a multilevel world. *Ecology and society, 11*(2).
Cavalieri, F., Franchin, P., Buriticá Cortés, J. A., & Tesfamariam, S. (2014). Models for seismic vulnerability analysis of power networks: comparative assessment. *Computer-Aided Civil and Infrastructure Engineering, 29*(8), 590-607.
Cavalieri, F., Franchin, P., & Pinto, P. E. (2014). Fragility functions of electric power stations *SYNER-G: typology definition and fragility functions for physical elements at seismic risk* (pp. 157-185): Springer.
Cimellaro, & Marasco, S. (2015). A computer-based environment for processing and selection of seismic ground motion records: OPENSIGNAL. *Frontiers in Built Environment, 1*, 17.
Cimellaro, Ozzello, F., Vallero, A., Mahin, S., & Shao, B. (2017). Simulating earthquake evacuation using human behavior models. *Earthquake Engineering & Structural Dynamics, 46*(6), 985-1002. doi:10.1002/eqe.2840
Cimellaro, Renschler, C., Reinhorn, A. M., & Arendt, L. (2016). PEOPLES: a framework for evaluating resilience. *Journal of Structural Engineering, ASCE, 142*(10), 1-13 DOI: 10.1061/(ASCE)ST.1943-1541X.0001514. doi:http://dx.doi.org/10.1061/(ASCE)ST.1943-541X.0001514
Cimellaro, G. P. (2016). Urban resilience for emergency response and recovery. *Switzerland: Springer [DOI: 10.1007/978-3-319-30656-8]*.
Cimellaro, G. P., Mahin, S., & Domaneschi, M. (2019). Integrating a Human Behavior Model within an Agent-Based Approach for Blasting Evacuation. *Computer-Aided Civil and Infrastructure Engineering, 34*(1), 3-20.
Cimellaro, G. P., Ozzello, F., Vallero, A., Mahin, S., & Shao, B. (2017). Simulating earthquake evacuation using human behavior models. *Earthquake Engineering & Structural Dynamics, 46*(6), 985-1002.
Crowley, H., Pinho, R., Pagani, M., & Keller, N. (2013). Assessing global earthquake risks: the Global Earthquake Model (GEM) initiative *Handbook of seismic risk analysis and management of civil infrastructure systems* (pp. 815-838): Elsevier.
Cutter, S. L., Barnes, L., Berry, M., Burton, C., Evans, E., Tate, E., & Webb, J. (2008). A place-based model for understanding community resilience to natural disasters. *Global Environmental Change, 18*(4), 598–606.
De Iuliis, M., Kammouh, O., Cimellaro, G. P., & Tesfamariam, S. (2019). Downtime estimation of building structures using fuzzy logic. *International Journal of Disaster Risk Reduction, 34*, 196-208. doi:https://doi.org/10.1016/j.ijdrr.2018.11.017
DEEDS. Digital Environment for Enabling Data-Driven Science. Retrieved from https://datacenterhub.org/
Ding, Y., Zhu, Q., & Lin, H. (2014). An integrated virtual geographic environmental simulation framework: a case study of flood disaster simulation. *Geo-spatial Information Science, 17*(4), 190-200.
Domaneschi, M., Cimellaro, G. P., & Scutiero, G. (2019). A simplified method to assess generation of seismic debris for masonry structures. *Engineering Structures, 186*, 306-320.

Dudenhoeffer, D. D., Permann, M. R., & Manic, M. (2006). *CIMS: A framework for infrastructure interdependency modeling and analysis.* Paper presented at the Proceedings of the 38th conference on Winter simulation.

EERI. The Earthquake Engineering Research Institute collection of case studies. Retrieved from http://db.concretecoalition.org/

Eidinger, J., Avila, E., Ballantyne, D., Cheng, L., Der Kiureghian, A., Maison, B., . . . Power, M. (2001). Seismic fragility formulations for water systems. *sponsored by the American Lifelines Alliance, G&E Engineering Systems Inc., web site http://homepage.mac.com/eidinger*.

Fujisaki, E., Takhirov, S., Xie, Q., & Mosalam, K. M. (2014). *Seismic vulnerability of power supply: lessons learned from recent earthquakes and future horizons of research.* Paper presented at the Proceedings of 9th international conference on structural dynamics (EURODYN 2014). European Association for Structural Dynamics, Porto, Portugal.

GEER. Geotechnical Extreme Events Reconnaissance. Retrieved from http://www.geerassociation.org/

Ghobarah, A. (2004). *On drift limits associated with different damage levels.* Paper presented at the International workshop on performance-based seismic design.

Guidotti, R., Chmielewski, H., Unnikrishnan, V., Gardoni, P., McAllister, T., & van de Lindt, J. (2016). Modeling the resilience of critical infrastructure: The role of network dependencies. *Sustainable and resilient infrastructure, 1*(3-4), 153-168.

Hagberg, A., Swart, P., & S Chult, D. (2008). *Exploring network structure, dynamics, and function using NetworkX*. Retrieved from

Haklay, M., & Weber, P. (2008). Openstreetmap: User-generated street maps. *IEEE Pervasive Computing, 7*(4), 12-18.

Hwang, S., Park, M., Lee, H.-S., & Lee, S. (2016). Hybrid simulation framework for immediate facility restoration planning after a catastrophic disaster. *Journal of Construction Engineering and Management, 142*(8), 04016026.

Ismail, M. A., Sadiq, R., Soleymani, H. R., & Tesfamariam, S. (2011). Developing a road performance index using a Bayesian belief network model. *Journal of the Franklin Institute, 348*(9), 2539-2555.

ISTAT, A. S. I. (2016). Istituto Nazionale di statistica.

Kammouh, O., Cimellaro, G. P., & Mahin, S. A. (2018). Downtime estimation and analysis of lifelines after an earthquake. *Engineering Structures, 173*, 393-403. doi:https://doi.org/10.1016/j.engstruct.2018.06.093

Kammouh, O., Noori, A. Z., Cimellaro, G. P., & Mahin, S. A. (2019). Resilience Assessment of Urban Communities. *ASCE-ASME Journal of Risk and Uncertainty in Engineering Systems, Part A: Civil Engineering, 5*(1), 04019002. doi:doi:10.1061/AJRUA6.0001004

Kammouh, O., Noori, A. Z., Taurino, V., Mahin, S. A., & Cimellaro, G. P. (2018). Deterministic and fuzzy-based methods to evaluate community resilience. *Earthquake Engineering and Engineering Vibration, 17*(2), 261-275. doi:10.1007/s11803-018-0440-2

Karakoc, D. B., Barker, K., Zobel, C. W., & Almoghathawi, Y. (2020). Social Vulnerability and Equity Perspectives on Interdependent Infrastructure Network Component Importance. *Sustainable Cities and Society*, 102072.

Kirk, D. (2007). *NVIDIA CUDA software and GPU parallel computing architecture.* Paper presented at the ISMM.

Latora, V., & Marchiori, M. (2001). Efficient behavior of small-world networks. *Physical review letters, 87*(19), 198701.

Liaw, A., & Wiener, M. (2002). Classification and regression by randomForest. *R news, 2*(3), 18-22.

Lu, X., & Guan, H. (2017). *Earthquake disaster simulation of civil infrastructures*: Springer.

Maguire, D. J. (1991). An overview and definition of GIS. *Geographical information systems: Principles and applications, 1*, 9-20.

Marasco, S., Noori, A. Z., & Cimellaro, G. P. (2017). Resilience Assessment for the Built Environment of a Virtual City. *compdyn 2017 Proceedings*, 1-13.

Martí, J. R. (2014). Multisystem simulation: analysis of critical infrastructures for disaster response *Networks of networks: the last frontier of complexity* (pp. 255-277): Springer.

Mazzoni, S., McKenna, F., Scott, M. H., & Fenves, G. L. (2006). OpenSees command language manual. *Pacific Earthquake Engineering Research (PEER) Center, 264*.

Mirza, S. A., & MacGregor, J. G. (1979). Variability of mechanical properties of reinforcing bars. *Journal of the Structural Division, 105*(ASCE 14590 Proceeding).

Ni, K. S., & Nguyen, T. Q. (2009). An adaptable $ k $-nearest neighbors algorithm for MMSE image interpolation. *IEEE transactions on image processing, 18*(9), 1976-1987.

Noori, A. Z., Marasco, S., Kammouh, O., Domaneschi, M., & Cimellaro, G. (2017). *Smart cities to improve resilience of communities.* Paper presented at the 8th International Conference on Structural Health Monitoring of Intelligent Infrastructure.

Ouyang, M. (2014). Review on modeling and simulation of interdependent critical infrastructure systems. *Reliability engineering & System safety, 121*, 43-60.

Pamungkas, A., Bekessy, S. A., & Lane, R. (2014). Vulnerability modelling to improve assessment process on community vulnerability. *Procedia-Social and Behavioral Sciences, 135*, 159-166.

Piegl, L. A., & Tiller, W. (2002). Algorithm for finding all k nearest neighbors. *Computer-Aided Design, 34*(2), 167-172.

Porter, K., Farokhnia, K., Cho, I., Grant, D., Jaiswal, K., Wald, D., & Noh, H. (2012). *Global vulnerability estimation methods for the global earthquake model.* Paper presented at the 15th World Conference on Earthquake Engineering, Lisbon, Portugal.

Prettico, G., Gangale, F., Mengolini, A., Lucas, A., & Fulli, G. (2016). Distribution System Operators Observatory. *European Commission. Joint Research Centre*.

Renschler, C. S., Frazier, A. E., Arendt, L. A., Cimellaro, G. P., Reinhorn, A. M., & Bruneau, M. (2010). *A framework for defining and measuring resilience at the community scale: The PEOPLES resilience framework*: MCEER Buffalo.

Repetto, M. P., Burlando, M., Solari, G., De Gaetano, P., & Pizzo, M. (2017). Integrated tools for improving the resilience of seaports under extreme wind events. *Sustainable Cities and Society, 32*, 277-294.

Ribeiro, P. J. G., & Gonçalves, L. (2019). Urban resilience: A conceptual framework. *Sustainable Cities and Society*, 101625.

Rossman, L. A. (2000). EPANET 2: users manual.

Silva, V., Crowley, H., Pagani, M., Monelli, D., & Pinho, R. (2014). Development of the OpenQuake engine, the Global Earthquake Model's open-source software for seismic risk assessment. *Natural Hazards, 72*(3), 1409-1427.

Svennerberg, G. (2010). *Beginning Google Maps API 3*: Apress.

Takeda, T., Sozen, M. A., & Nielsen, N. N. (1970). Reinforced concrete response to simulated earthquakes. *Journal of the Structural Division, 96*(12), 2557-2573.

Taurino, V., Kammouh, O., Cardoni, A., & Paolo, G. (2018). RESILIENCE ASSESSMENT OF LARGE SCALE WATER DISTRIBUTION NETWORKS: A SIMULATION APPROACH.

UnityTechnologies. (2020). Unity. Retrieved from https://unity.com/

Vrouwenvelder, T., & Faber, M. (2001). Probabilistic model code. *Joint Committee on Structural Safety, website http://www.jcss.ethz*.

Walker, B., & Salt, D. (2006). The system rules: creating a mind space for resilience thinking. *Walker, B. and Salt, D. Resilience Thinking: Sustaining Ecosystems and People in a Changing World. Island Press, Washington*, 28-52.

Yang, Y., Ng, S. T., Zhou, S., Xu, F. J., & Li, H. (2019). Physics-based resilience assessment of interdependent civil infrastructure systems with condition-varying components: A case with stormwater drainage system and road transport system. *Sustainable Cities and Society*, 101886.

Yao, B., Khosla, A., & Fei-Fei, L. (2011). *Combining randomization and discrimination for fine-grained image categorization.* Paper presented at the CVPR 2011.

Zhu, M., McKenna, F., & Scott, M. H. (2018). OpenSeesPy: Python library for the OpenSees finite element framework. *SoftwareX, 7*, 6-11.